Structural connectome quantifies tumor invasion and predicts survival in glioblastoma patients

Abstract

Background

Glioblastoma is characterized by extensive invasion into brain parenchymal tissue through white matter tracts. Systematically quantifying invasion, however, is limited by the conventional imaging tools, and could potentially be achieved by a structural connectome approach.

Methods

Two prospective patient cohorts of newly diagnosed glioblastoma were included for network construction. A fiber template was firstly derived by employing probabilistic tractography on healthy subjects. Through performing tract-based spatial statistics in patients and age-matched controls, the connectivity strength of each fiber was estimated in patients for network construction. Contrast-enhancing and non-enhancing tumors were segmented and overlaid to the network to identify connectome disruption in lesion and distant areas. The connectome disruption probabilities were calculated across all patients. Disruption indices and network topological features were examined using survival models.

Results

The distant areas accounted for higher proportion of disruption than the contrast-enhancing tumor (16.8 ± 12.0% vs 5.8 ± 5.1%, $P < 0.001$). Compared to healthy controls, patient networks demonstrated lower clustering coefficient, but higher characteristic path length (each $P < 0.001$). Higher distant area disruption (HR = 1.43, $P = 0.027$) and characteristic path length (HR = 1.59, $P = 0.031$) were associated with worse survival, while higher clustering coefficient (HR = 0.59, $P = 0.016$) was associated with prolonged survival.

Conclusion

The occult invasion in glioblastoma could be identified and quantified using structural connectome, which may confer benefits to precise patient management.

Keywords: tumor invasion, structural connectome, glioblastoma, diffusion imaging, survival

Introduction

Glioblastoma is the most common primary malignant brain tumor in adults (1), characterized by its diffuse invasion along the white matter tracts (2), whereby tumor cells diffusely invade the brain. It is increasingly accepted that glioblastoma should be considered as a *systematic* disease (3-5). The conventional imaging, however, cannot identify the tumor invasion across the whole brain. As glioblastoma patients generally demonstrate remarkable variability, there is a pressing need to stratify patients more accurately for individualized treatment. This crucial clinical demand could be potentially achieved by *systematically* quantifying tumor invasion.

Diffusion MRI (dMRI) is a method that infers the microstructure of white matter tract by measuring water mobility. It is more sensitive at detecting occult tumor invasion, compared to the structural T1-weighted and FLAIR imaging (6). Evidence shows that the dMRI characteristics of glioblastoma is correlated with the histology of biopsied tissue (7,8). In glioblastoma, dMRI has been used to evaluate tumor invasiveness, detect invasion in the peritumoral infiltrated region, and identify phenotypes that are correlated with IDH mutation status (9-13). It also offers value for the determination of subventricular zone involvement in glioblastoma (14,15). These analyses, however, have focused on the *regional invasion* instead of the *systematic disturbance* in glioblastoma.

Recently, network analysis using the graph theory has shown its promises in characterizing various neurological and psychiatric disorders based on dMRI (16-19). Using this approach, the brain structure can be represented as a complex network, namely structural connectome, where the connectivity among cortical/subcortical brain regions is measured by the connecting tracts (20). Further, graph theoretical analysis can facilitate the characterization of connectome topology (21,22). Recent studies suggest that brain tumors may alter the topological organization of structural connectome (23-25). Additionally, the

topological features derived from the structural connectome appear to outperform clinical parameters for survival prediction in preliminary studies (26). However, these findings are based on small numbers of patients and require further evaluation in larger cohorts for clinical evidence. Moreover, it remains largely unknown whether the tumor-induced disruption in the brain structural connectome could be quantified, with intra-tumor heterogeneity sufficiently addressed. Of particular significance is the prognostic value of structural connectome in glioblastoma patients for more precise management stratification.

The purpose of this study was to characterize the disruption of the structural connectome and further investigate its prognostic value using two larger prospective glioblastoma cohorts. We hypothesized that glioblastoma could induce both focal and global structural network disturbance, which could be associated with tumor invasion and impact patient outcomes. To test this hypothesis, firstly we constructed structural networks using dMRI from glioblastoma patients and healthy controls. Secondly, the focal and distant disrupted connectome were quantified separately from each individual patient. Finally, the disruption indices and topological features were calculated and examined in survival models. Two prospective glioblastoma cohorts were evaluated separately for cross validation,

Methods

Study design

The schematic representation of the study design is summarized in **Figure 1**. Directly performing tractography in the lesioned brain may cause artefacts, e.g., an unrealistic belt of fibers surrounding the tumor core.(27),(28) Previous evidence shows that the white matter integrity in glioma patients can be quantitatively assessed using the fractional anisotropy (FA), a robust measure derived from dMRI, after applying the deformable nonlinear registration (29-31). Further studies showed that the tract integrity of the lesioned brain can be estimated by using the tract templates derived from healthy controls (32-34), and the alignment-invariant tract representation (FA skeleton) generated using the tract-based spatial statistics (TBSS) (35). This method has yielded robust estimation of network connectivity in the lesioned brain (27,34,36).

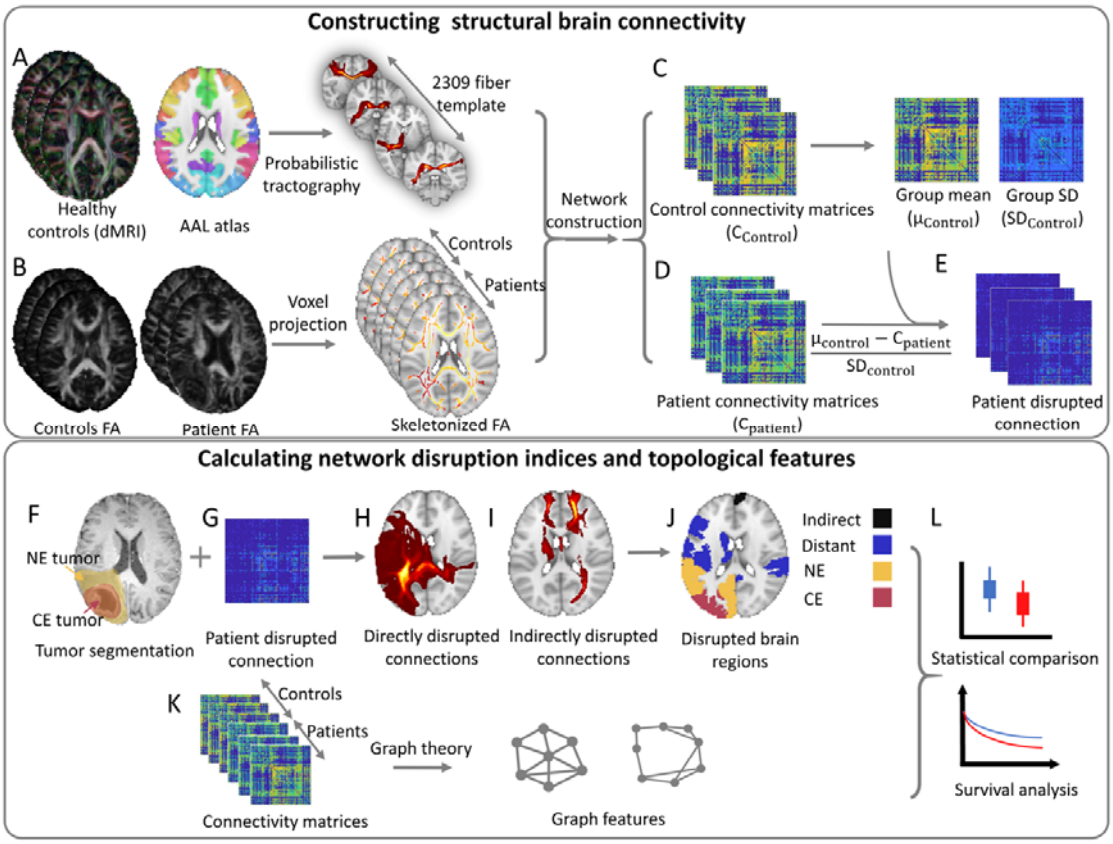

Figure 1 Study overview. (A). Probabilistic tractography was performed on dMRI of ten healthy controls between 90 separate brain regions defined by anatomical atlas AAL to generate tractography template for the prior knowledge of anatomical connections of white matter tracts. (**B).** Skeletonize FA map of both patients and another cohort of healthy controls were generated using TBSS protocols. **(C).** The patients/controls connectivity matrices are computed by averaging the segments of FA skeleton within each tract of tractography template between each pair of brain regions, representing the strength of white matter connections. The connectivity disruption **(E)** was defined as the SD normalized decreases in connectivity of patient **(D)** comparing to the group mean connectivity of controls**.** If the connectivity in patient is 2SD lower than mean connectivity, the connection was defined as significantly disrupted with 95% confidence. **(F)** Tumor were segmented into contrasting enhancing tumor (CE, red) and non-enhancing tumors (NE, yellow). The significantly disrupted white matter connections were further classified as tumor disrupted white matter connections **(G)** and indirectly disrupted white matter connections **(H)** . Furthermore, the AAL defined brain regions were further classified into CE, NE, Distant and Indirect disrupted brain regions **(I)**, depending on what tumor segment infiltrated the areas or whether the brain regions were linked by the disrupted connections within tumor. (**J).** Connectivity matrices of both patients and controls were both thresholded to produce robust topological features of clustering coefficient and characteristic path length. **(K).** The prognostic relevance of the white matter disruption and topological features were investigated in survival models.

Subjects

This study was approved by the local institutional review board. Informed written consent was obtained from all patients. Healthy controls data were obtained from two open-source datasets with ethical approval.

Glioblastoma patients. Patients with a radiological diagnosis of *de novo* supratentorial glioblastoma were prospectively recruited for surgical resection (Discovery cohort: July 2010 - August 2015; Validation cohort: July 2017 - October 2019) by the multidisciplinary team (MDT) central review. Patients were included in both cohorts following identical inclusion and exclusion criteria (see Supplementary methods for detailed criteria). For both cohorts, patients were consecutively recruited, with data prospectively collected.

Patient pre-operative cognitive performance was tested using the Mini-Mental State Examination (MMSE) in the Discovery cohort. The MMSE score was dichotomized as <27 or >=27 according to a previous study (37). All glioblastoma patients underwent preoperative 3D MPRAGE (pre-contrast [T1] and post-contrast [T1C]), T2-weighted FLAIR, and dMRI sequences.

Healthy subjects for high spatial resolution tractography template. Ten age-matched healthy controls (6 males, mean age 60.9 years) were selected from the Alzheimer's disease Neuroimaging Initiative (ADNI, http://adni.loni.usc.edu/) for constructing an unbiased high spatial resolution tractography template. High angular resolution dMRI (54 directions, b value = 1000 s/mm^2) and T1 sequences were downloaded from ADNI.

***Age mathched healthy controls*.** Another healthy control cohort of 117 age matched subjects (mean age 59.9 years) was included to generate healthy control brain networks. The dMRI

(15 directions, b value =1000 s/mm^2) and T1 sequences were downloaded from https://brain-development.org/ixi-dataset/. The scanning protocols for all subjects are detailed in Supplementary Methods.

Treatment

All patients underwent maximal safe surgery using 5-aminolevulinic acid fluorescence (5-ALA, Medac, Stirling, UK) and neuro-navigation (StealthStation, Medtronic, Fridley, MN, USA). The extent of resection (EOR) was assessed according to the post-operative MRI within 72 hours as complete or partial resection of enhancing tumor or biopsy. Adjuvant therapy was determined by the MDT, according to the standard treatment protocols based on the patient post-operative status. All patients were followed up after surgery according to the criteria of response assessment in neuro-oncology (RANO). Overall survival (OS) and progression-free survival (PFS) were used as the primary endpoints.

Tumor segmentation

All anatomical MRI for tumor segmentation including T1, T2 and FLAIR were co-registered to T1C images with an affine transformation, using the linear image registration tool (FLIRT) functions in the FMRIB Software Library (FSL)(38). To segment the tumor, we applied a multi-scale 3D Deep Convolutional Neural Network (39), implemented in the Cancer Imaging Phenomics Toolkit (CaPTk) (https://cbica.github.io/CaPTk/index.html). Manual correction was performed using 3D slicer v4.6.2 (https://www.slicer.org/), by a neurosurgeon (XX) and a researcher (XX) after an initial training period and reviewed by an experienced neuroradiologist (XX). The final consensus was achieved using the Dice score to ensure inter-rater reliability. Finally, tumors were segmented into the contrast-enhancing tumor mask (CE mask, red) and non-enhancing mask (NE mask, yellow), representing the complete

region within the contrast-enhancing rim on post-contrast T1 and FLAIR hyperintensities surrounding the CE, respectively (**Figure 1I**).

Network construction

The complete pipeline of network construction includes three steps: 1) constructing group tractography template, 2) producing individualized skeletonized FA map, 3) combining the tractography template and FA skeleton to produce connectivity matrices.

Tractography template. An unbiased tractography template in standard space was generated using the probabilistic tractography in dMRI of healthy controls.

1) Cortical/subcortical brain areas of dMRI were parcellated into 90 region of interest (ROIs) according to Automatic Anatomical Labeling (AAL) atlas (40) in standard MNI-152 space (41) (**Figure 1A**). Both linear and deformable registration were performed using the Advanced Normalization Tools (ANTs) (42). AAL atlas includes gray-white matter boundary to facilitate tractography.

2) Eddy currents and subject motions in dMRI were corrected using the FSL eddy tool (version 6.0.0). A crossing fiber model was then fitted to each control's dMRI using the FSL function bedpostx. Probabilistic tractography between each pair of the 90 ROIs was subsequently performed using FSL Probtrackx2 (43). Each ROI was used as a seed (starting ROI) or target (ending ROI) once for tracking. For each pair of seed/target ROIs, 5000 streamlines were sampled from the seed mask, only the streamlines reached the target mask were retained. The tracking curvature threshold was set to 0.2 (80 degrees). Streamline samples were terminated when they have travelled 2000 steps with step length of 0.5mm or entered the cortical/subcortical brain regions. Streamlines were discarded if they entered the cerebrospinal fluids (CSF) in ventricle or re-entered the seed region.

3) For each control, fiber path distribution maps were generated for all possible connections between the 90 cortical/subcortical brain regions. The fiber path distribution maps of all healthy controls were then nonlinearly transformed back to the MNI-152 standard T1 space using ANTs and averaged to a mean fiber path distribution across controls using function fslmaths. The mean path distribution was then thresholded and binarized, such that only the voxels with top 5% obability in the fiber were retained, providing a conservative pathway for the tracography template (**Figure 1B**).

Skeletonized FA map. To mitigate partial-volume effect, skeletonized FA maps were generated for estimating the patient individual tract connectivity strength by following TBSS protocols (35). Age-matched healthy subjects were selected controls to reduce the bias from aging-related white matter pathology.

After the same preprocessing protocols of dMRI as the tractography templates. The dMRI were fitted with a tensor model to produce FA map using the FSL diffusion toolbox (FDT)(44). The FA maps were then non-linearly co-registered to the MNI-152 space FA template using the deformable function SYN of ANTs. (**Figure 1C**)

ANTs was shown to outperform the default deformable registration tools FNIRT (45) of TBSS in the co-registration of FA (46) and pathology-bearing T1 images (47), and more importantly could mitigate the deformation of the brains with tumor by accounting for the tumor mass effect (48). To minimize the bias of signal-noise ratio introduced by the different MRI acquisition protocols, we normalized the FA map using the MRI intensity histogram-matching method(49).

The standard TBSS protocol was followed to produce a skeletonized FA map for each subject. First, a mean FA was generated by averaging all the FA map of patients and controls in the standard space. Second, a study-specific FA skeleton mask representing the common centers of tracts for all subjects was produced by thinning the group mean FA map followed by binarization. Finally, the local maxima FA voxels from each patient FA map were projected to this skeleton to produce individualized whole-brain skeletons. (**Figure 1D**)

Constructing connectivity matrices. The connectivity matrix or brain network for each patient and control was estimated as the mean value of the tract segments in the individualized FA skeleton, constrained by the tractography template. (**Figure 1F, G**)

The columns and rows of each individualized connectivity matrix represent the brain regions in AAL atlas, while the elements in the matrices (W_{ij}) represent the strength of white matter connection between the brain regions *i* and *j*. According to the graph theory, we calculated the strength S_i for area *i* by aggregating the connectivity strength of white matter connection W_{ij} that connected to brain regions *i*, as the below formula:

$$S_i = \sum_{j \neq i} W_{ij}$$

In this way, the disruptions of thousands of white matters fibers can be summarized on 90 brain areas. Additionally, impacts on brain regions can also be captured by the disruptions of white matter fibers connecting to them.

To evaluate the robustness of the network constructed using the dMRI acquired from different protocols, we further compared the connection strengths of a cerebellar tract in the two patient cohorts, where this tract is not affected by the supratentorial tumors,

Identification of significantly disrupted connectome

To identify white matter connection disruptions in tumor patients, we firstly calculated the mean and SD of the strength of each connection in healthy controls. Then, for patient individualized network, we compare every connection strength with the mean connection strength in controls. The significantly decreased connection in patients is defined as a connection that is 2SD lower than the mean connection strength in controls, where 2SD indicates 95% confidence (**Figure 1G, H**). Similarly, the significant threshold for the disruptions of AAL brain regions was also defined as 2SD.

Identification of regional disrupted connectome

To address the intra-tumor heterogeneity, we categorized the disrupted white matter connections and brain regions as below (**Figure 1I, 1K and 1L**):

1. Disrupted white matter connections

1) **Tumor disrupted connections:** connections that are directly disrupted by tumor, which travel cross the contrasting enhancing or non-enhancing tumor.
2) **Indirect disrupted connections:** connections that are disrupted without crossing the lesion area.

2. Disrupted brain regions

1) **Tumor disrupted areas:** the AAL brain regions that are within the tumor region and directly disrupted by tumor. These areas were further categorized into the **CE-disrupted** or **NE-disrupted areas,** depending on overlapping between tumor and AAL brain regions.
2) **Distant disrupted areas:** disrupted brain regions within the normal-appearing brain and connected to the tumor via white matter connections.

3) **Indirect disrupted areas:** disrupted brain regions without any connections linked to the tumor.

To increase the specificity of this methods, we calculated the disruption of each connection/area category as a disruption index by averaging the SD scaled decreases separately and generated five disruption indices for each patient.

Topological features of structural network

Topological features were calculated using the Brain Connectivity Toolbox (22). We filtered the connectivity matrix to remove the connections with changes of more than 2SD, as topological features are sensitive to noise. To specifically investigate the tendency of segregation and integration of the brain network under the attack of tumor, we calculated the clustering coefficient (segregation) and characteristic path length (integration) (50). Briefly, the clustering coefficient measures the probability of two direct topological neighbors of a specific brain regions also being connected. The characteristic path length measures the average shortest path length of the brain network, which is also the inverse of global efficiency of the brain network. (see Supplementary Methods for detailed definition). (**Figure 1 M, N and O**)

Statistical analysis

All analyses were performed in RStudio v3.2.3 (RStudio, Boston, USA) and MATLAB 2019b (The MathWorks Inc). The disruption indices, the topological features of subjects, and the cognitive groups defined by MMSE were compared respectively using the two-sample t-test. Pearson correlation was tested between each pair of disruption indices. Multiple comparisons were adjusted by false discovery rate (FDR).

Survival analysis was performed using OS and PFS as the endpoints. Patients who were alive at the last known follow-up were censored. Disruption indices or topological features were dichotomized according to either median or the optimal cut-off value defined using the maximally selected rank statistics in the R package 'Survminer' (51), whichever was more significant. Kaplan-Meier survival curves were compared using the log-rank test.

Cox proportional hazards regression accounted for all relevant clinical covariates, including O-6-methylguanine-DNA methyltransferase (MGMT) methylation status, isocitrate dehydrogenase-1 (IDH-1) mutation, sex, age, extent of resection, adjuvant therapy, tumor volume. We also included two features from the VASARI feature set describing the involvement of eloquent cortex and deep white matter (52), in order to account for the effects of tumor cortical/subcortical brain regions. (**Figure 1P**)

Receiver operating characteristic (ROC) curves were used to evaluate the accuracy of predicting the OS, using the significant variables in the univariate models. To evaluate the prognostic values of tumor disruption and topological features, a generalized linear models were fitted to calculate the area under the curve (AUC). The hypothesis of no effect was rejected at a two-sided level of 0.05.

Results

Patient population

Table 1 presents the summary of two study cohorts (See Supplementary Methods for a flowchart of patient inclusion). For the Discovery cohort, a total of 136 patients were recruited for pre-operative MRI scanning. After excluding 19 patients, 117 of 136 (86.0 %) patients (mean age 59 years, range 22-75 years, 89 males) were included. Six patients (5.1 %) were lost in follow up. The median OS was 392 (range 34-1932; CI 317- 426) days.

For the Validation cohort, a total of 49 patients were initially recruited. After excluding seven patients using identical criteria, 42 of 49 (85.7 %) patients (mean age 61 years, range 28-75 years, 34 males) were included. The median OS was 335 (range 55- 962; CI 245- 497) days.

No significant differences were found between the two study cohorts regarding the clinical characteristics.

Table 1. Summary of the patient cohorts

Variable	Patient Number		*P*
	Training	Validation	
Age at diagnosis			
<60	42	18	0.425
≥60	75	24	
Sex			
Male	89	30	0.236
Female	28	12	
Extent of resection (of enhancing tumor)			
Complete	77	32	0.572
Partial	32	6	
Biopsy	8	4	
MGMT-methylation status [a]			
Methylated	49	21	0.363
Unmethylated	68	21	
IDH-1 mutation status			
Mutant	7	1	0.360
Wild type	110	41	
Pre-operative Tumor volumes(cm^3) [b]			
Contrast-enhancing	44.7 ± 28.8	45.2 ± 29.4	0.841
Non-enhancing	50.3 ± 36.2	46.4 ± 32.6	0.652

(a) MGMT-methylation status unavailable for 4 patients; (b) mean ± SD of original data. MGMT: O-6-methylguanine-DNA methyltransferase; IDH-1: Isocitrate dehydrogenase 1.

The Peritumoral region showed similar extent of disruption with core tumor

Figure 2 presents an example of significantly disrupted white matter connections and brain regions, with the CE and NE tumor regions labeled. The disruption indices of two study cohorts showed no significant difference (**Supplementary Table S1**), suggesting the robustness of the indices.

In the regional comparisons (**Figure 2A & B**, **Supplementary Table S2**), focal tumor disruptions on white matter connections (4.77 ± 1.56) exhibited higher extent of disruption than the indirect disruptions of white matter connections in normal-appearing brain (3.11 ± 0.43, P <0.001). Similarly, focal tumor disrupted brain regions (CE: 5.83 ± 2.00; NE: 4.67 ± 1.33) had higher disruption than the normal-appearing brain (Distant: 2.90 ± 0.71, Indirect: 2.56 ± 0.39, each P <0.001).

Pearson correlation tests showed that the brain regions disruption of CE and NE regions were correlated (CE vs NE: r = 0.41, P < 0.001). The disruption of Distant brain areas was correlated with the disruptions of the brain regions that are inside tumor regions (CE vs Distant: r = 0.43, P <0.001; NE vs Distant: r = 0.34, P = 0.015, **Supplementary Table S3**, **Supplementary Figure S1**).

The contrast-enhancing tumor volume was correlated with the Tumor disruption of white matter connections (r = 0.52, P < 0.001). Notably, the tumor volume was also correlated with the Distant disruption of brain regions (r = 0.33, P < 0.001, **Supplementary Table S11**, **Supplementary Figure S1**).

The normal-appearing brain showed widespread connectome disruptions

A higher number of Distant disruptions of brain regions (16.8 ± 12.0%) were identified from the normal-appearing brain, compared to the enhancing lesion (CE disruptions of brain

regions: 5.8 ± 5.1%, $P < 0.001$, **Supplementary Figure S2C**). The above findings were recapitulated by the Validation cohort (**Supplementary Table S4** and **Figure S2B & D**).

Topological features could reflect tumor-induced connectome impairment

The topological features of both study cohorts showed significant decreases comparing to healthy controls (**Supplementary Table S7** and **Figure S5**). Particularly, the clustering coefficient of the patient structural network was significantly lower than healthy controls ($P < 0.001$). In contrast, the characteristic path length of the patient network was significantly higher than healthy controls ($P < 0.001$). The above results may suggest the tumor lesion may scientifically alter the network topology.

Further, we compared the topological features of the patient subgroups stratified using MMSE score. The results showed that the patient subgroup with lower MMSE score had higher characteristic path length (P = 0.012) and lower clustering coefficient (P = 0.007).

All topological features were significantly correlated with tumor volume (clustering coefficient r = -0.45, characteristic path r = 0.43; each P < 0.001), which suggests the larger impacts from the greater size of the focal lesion to the network topology.

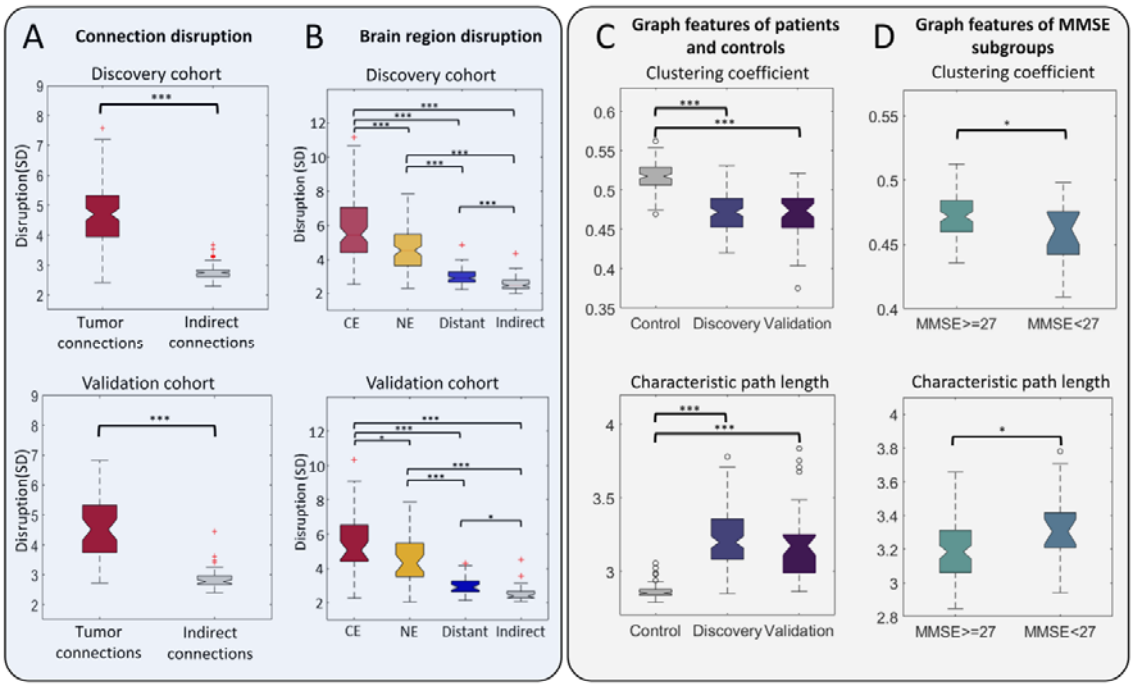

Figure 2 Feature statistics. (A-B) Different brain regions disruption comparison in Discovery and Validation cohort **(C)** Topological features comparison between controls and patients. **(D)** Topological features differed in patient groups of different cognitive status. (*P* value * <0.05, ** <0.005, ***<0.001)

Disruption indices of the normal-appearing brain showed prognostic value

We examined the prognostic significance of disruption indices and topological features separately in survival models (**Table 2**). For disruption indices, the univariate models showed that higher Indirect disruption of white matter connections (OS: HR = 1.36, *P* = 0.007; PFS: HR = 2.43, *P* = 0.046) and Distant disruptions of brain regions(OS: HR = 1.46, *P* = 0.049; PFS: HR = 1.49, *P* = 0.019) disruptions were significantly associated with worse OS and PFS. These two indices remained significant in the multivariate model adjusting for all the significant clinical covariates from the univariate model. Figure 3 presents the results of the multivariate models.

Table 2. Univariate survival statistics of Discovery cohort

Feature	OSN			PFSN		
	HR	95%CI	*P*	HR	95%CI	*P*
Clinical variables						
Age	1.03	1.01 -1.05	**0.004**	1.03	1.00-1.05	**0.021**
Sex[a]	0.81	0.52-1.25	0.333	0.75	0.47-1.19	0.217
Performance[b]	1.60	1.09-2.36	**0.018**	1.63	1.04-2.55	**0.033**
IDH[c]	0.59	0.25-1.36	0.211	0.52	0.22-1.21	0.131
MGMT[d]	0.77	0.52-1.14	0.196	0.68	0.43-1.07	0.094
EOR[e]	1.89	1.26-2.84	**0.002**	1.90	1.19-3.03	**0.007**
Adjuvant treatment[f]	0.21	0.13-0.34	**<0.001**	0.22	0.11-0.41	**<0.001**
Tumor volume	1.01	1.00-1.01	**0.001**	1.01	1.00-1.02	**0.045**
Eloquent location[g]	0.93	0.64-1.36	0.711	1.06	0.69-1.62	0.807
Deep white matter[h]	0.85	0.58-1.24	0.386	0.86	0.57-1.31	0.487
Disruption indices[I]						
Tumor (WM) [J]	1.07	0.87-1.30	0.790	1.08	0.88-1.32	0.464
Indirect (WM)	1.36	1.13-1.65	**0.007**	2.43	1.02-5.81	**0.046**
CE (brain regions) [K]	0.95	0.86-1.04	0.667	0.96	0.86-1.06	0.418
NE (brain regions)	1.01	0.88-1.15	0.939	1.00	0.87-1.15	0.979
Distant (brain regions)	1.46	1.08-1.99	**0.049**	1.49	1.07-2.07	**0.019**
Indirect (brain regions)	1.06	0.87-1.29	0.790	0.80	0.83-1.28	0.795
Topological feature[I]						
Clustering coefficient	0.63	0.42-0.93	**0.035**	0.49	0.30-0.78	**0.002**
Characteristic path length	1.56	1.06-2.29	**0.035**	1.82	1.16-2.84	**0.009**

(a). Female as the reference; (b). WHO Performance = 0 as the reference; (c). IDH wildtype as the reference; (d) Unmethylated MGMT as the reference; (e). Incomplete resection as the reference; (f) CCRT as the reference. (g). Non-eloquent location as reference. (h) Deep white matter tracts affected as reference. (I) All disruption indices and topological features were tested in turn by multivariate cox regression models that account for significant clinical variables in univariate cox regression. (J) Tumor (WM): Tumor disruptions of white matter connections. (K) CE (brain regions): CE lesion disruptions of brain regions

The Kaplan-Meier survival curves grouped by the mean value of the Distant disruption of brain regions (2.9 SD of decrease) showed that patients with higher disruption had a significantly worse survival (median 293 days) than those with lower Distant disruption of brain regions(median 449 days, log-rank, P = 0.002). The prognostic value of the Distant disruptions of brain regions was further confirmed by the Validation cohort (**Figure 4A**).

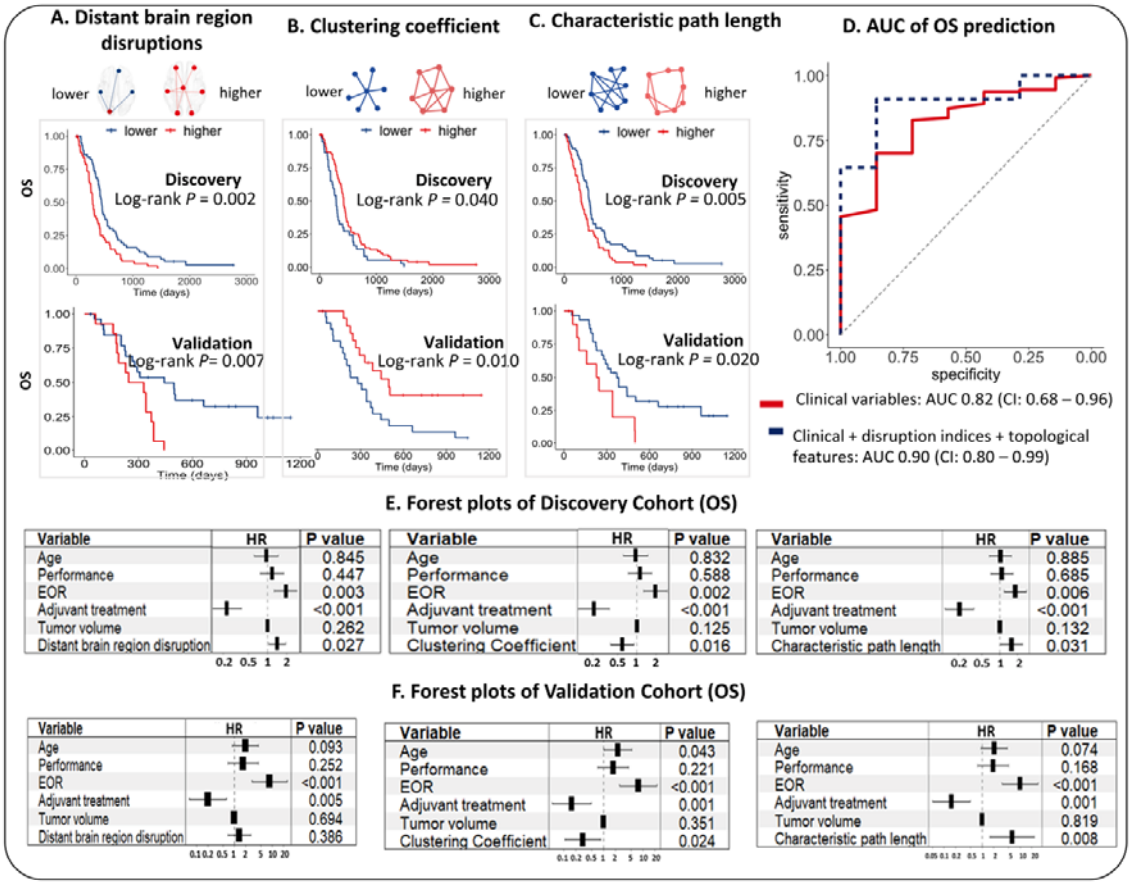

Figure 3 Survival analysis of overall survival in Discovery and Validation cohort. In both cohorts, higher Distant disruptions of brain regions (A), lower clustering coefficient (B), and higher characteristic path length (C) are associated with worse OS respectively. (D) The AUC of predicting 3-year OS using clinical factors, disruption indices, and topological features. (E-F) Prognosis values of most selected features remained when adding clinical variables. OS: Overall survival. HR: Hazard ratio

Topological features of the structural network showed prognostic significance

For topological features, the univariate models stratified by the optimal cut-offs showed that all the topological features were significantly associated with both OS and PFS. In the multivariate Cox model adjusting for all the significant clinical covariates from the univariate models, the derived patient subgroups were significantly associated with OS (clustering coefficient: HR = 0.63, P = 0.035; characteristic path length: HR = 1.77, P = 0.008) and PFS (clustering coefficient: HR = 0.49, P = 0.002; characteristic path length: HR = 1.82, P = 0.009) (**Table 2**). Kaplan-Meier survival curves demonstrated that topological features can

stratify patients into different survival groups (**Figure 4B & C**). Specifically, the group with clustering coefficient > 0.46 had better survival than the group with lower clustering coefficient (median 475 vs 294 days, log-rank, $P = 0.040$); the group with characteristic path length < 3.20 had better survival than the group with higher characteristic path length (median 465 vs 288 days, log-rank, $P = 0.005$). The prognostic significance of the topological features was further confirmed in the Validation cohort using the same models and thresholds (**Figure 4B & C**, **Supplementary Table S8**).

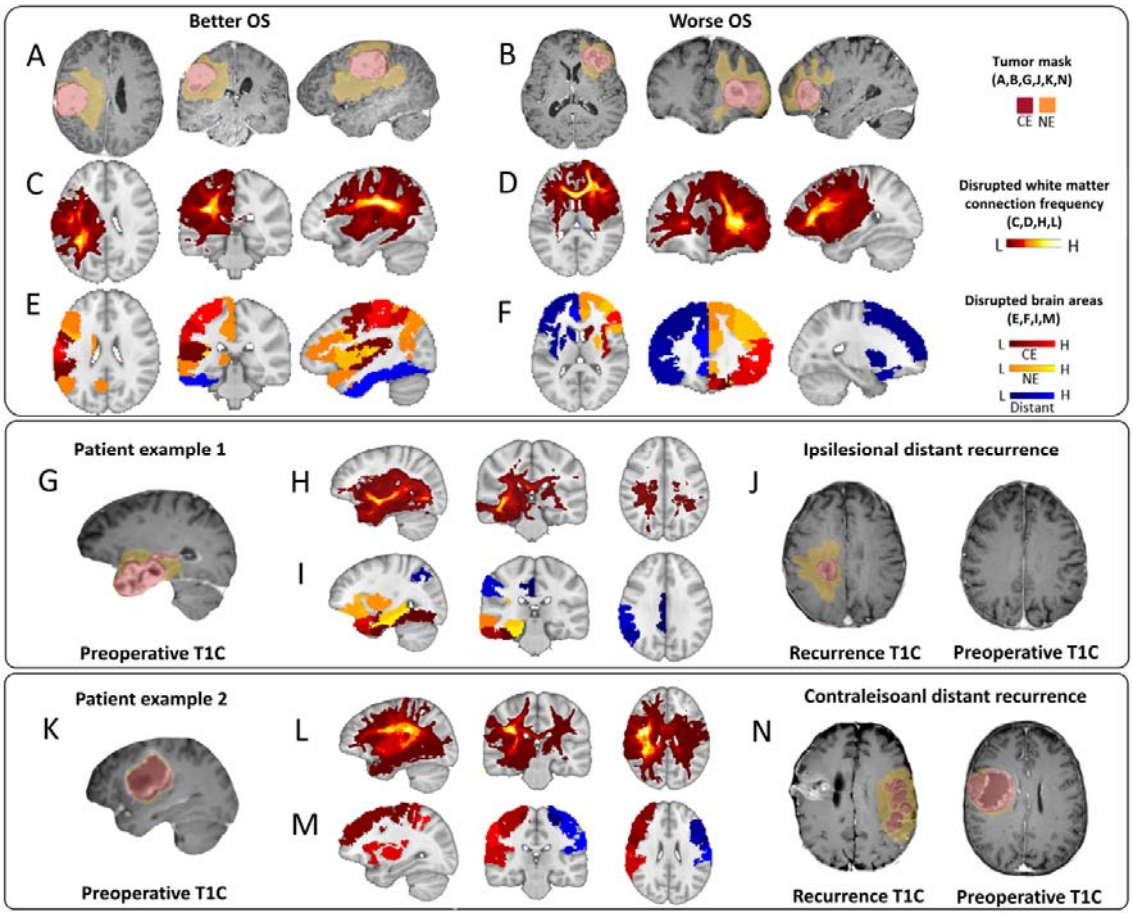

Figure 4 Prognostic value of disruption indices and topological features. (A-F) Case examples of better and worse OS (1555 vs 317 days). Both are IDH wildtype, MGMT unmethylated tumors in two male patients (aged 69 vs 67 years). They both underwent complete resection followed by TMZ chemoradiotherapy, with similar size of visible tumor (A, B) on post-contrast T1 (red) and FLAIR (yellow) images. (C, D) The probability maps of white matter disruption: (D) has more widespread disruption beyond the visible lesion, compared to (C); The disruption indices of Distant disruptions of brain regions (blue) are 2.8 (E) and 3.0 (F) respectively. Their topological features are distinct (c vs d: clustering coefficient 0.48 vs 0.44; characteristic path length 3.17 vs 3.31). (E-J) Case examples of patients with distant recurrence on the ipsilesional and contralesional brain hemisphere. (E, H) Pre-operative T1C on both patients. (F, I) Disrupted white matter connection frequency map. (G, J) Both distant recurrence sites are linked with original primary tumor via disrupted white matter connections.

Global connectome measures could enhance the performance of survival prediction

In the model of predicting OS, the baseline model including the significant clinical variables in the multivariate models, i.e., age, EOR, and adjuvant therapy, achieved AUC of 0.82 (CI: 0.68 - 0.96). By adding the significant disruption indices and topological features in the multivariate models, the AUC was improved at 0.90 (CI: 0.80 - 0.99, **Figure 3D**). We presented two example cases (**Figure 4E & F**) with distinct Distant disruptions of brain regions, topological features, and survival outcomes (above and below median respectively).

Discussion

The present study used a network approach to quantify the disruption of structural connectome in glioblastoma patients, and further validated its prognostic value for patient survival. Our main findings include: 1) glioblastoma can cause widespread disruption to both white matter tracts and brain areas, which is well beyond the focal region visualized on clinical routine scans. 2) The higher connectome disruption in the distant areas from the lesion is significantly correlated with worse patient survival. 3) A more topologically integrated structural network is significantly associated with better patient survival.

Glioblastoma is characterized by diffuse invasion into the parenchymal tissue. The normal-appearing brain is therefore considered as widely affected by the focal lesion. A systematic measurement is however limited by the commonly used analysis of focal voxels of interest. The network approach was proposed to solve this challenge, with the capability of modeling the structural connectivity of the entire brain, which allows the characterization of the systematically affected brain. This approach showed promises in almost all major neurological/psychiatric diseases.(16-19,33,34) Using resting-state fMRI, a previous study found that glioma could induce functional impairment in the distant areas from the lesion.(4,5) In this current study, we have shown glioblastomas may induce widespread structural impairment as well, which may be due to the systematic tumor invasion or Wallerian degeneration affecting normal-appearing regions.

To differentiate focal and distant disruptions, we separated the tumor into subregions and further quantified the disrupted connectome into multiple categories. Our results showed that the peritumoral NE region had a comparable extent of disruption with the core CE region, which is in agreement with the previous finding that tumor invasion is well beyond the enhancement margin.(53) The similar disruption probabilities of brain regionss from CE and NE corroborate this finding. Notably, although the disruption index of distant regions is

lower than the focal lesion, the disruption probabilities of these distant regions across the patient group are higher than the focal lesion. This could be the evidence of occult tumor invasion and explain the prognostic significance of the Distant disruptions of brain regions. The top distant areas with the highest disruption probability, e.g., posterior cingulate cortex and hippocampus, are important structures of the limbic system, suggesting that the occult invasion may preferably affect the limbic system. Moreover, as the top affected anatomical tracts, arcuate fasciculus and superior longitudinal fasciculus are important long association tracts widely connecting different separated gyri, suggesting that tumor invasion may widely spread along these tracts.

Another finding of the current study is that the topological features could provide a useful biomarker for patient stratification. By definition, the clustering coefficient reflects the segregation tendency of the network, while characteristic path length mainly reflects the network integration.(50) In the human brain, a balance between segregation and integration could be maintained.(54) The comparison between glioblastoma patients and healthy controls revealed that glioblastoma patients had decreased segregation and increased integration, which may indicate the network resilience under the tumor attack. Further, our results showed that a higher clustering coefficient and lower characteristic path length were associated with longer survival, suggesting a higher integration tendency in the impaired network that may resist the tumor disruption.

Our study has important clinical implications for glioblastoma patients. Due to the remarkable heterogeneity of glioblastoma, the development of quantitative prognostic markers is of crucial importance for precise diagnosis and treatment. By providing a global measure, structural connectome confers a novel approach to investigate the systematic changes of brain structure and function in glioblastoma patients. This approach could enable us to investigate not only the extent of disruption resulting from the tumor (tumor

aggressiveness) but also the extent that a lesioned brain could adapt or re-organize (network resilience). Understanding the interaction between the two perspectives could be equally crucial in the precise treatment of patients and the future development of novel therapeutics.

Our study has several limitations. Firstly, the structural connectome is only able to directly measure the white matter connectivity strength, using connecting tracts. Although the majority of brain areas are connected via white matter tracts, some functionally connected brain areas may not be structurally connected. Future work could be improved by adding resting-state MRI and functional connectivity. Secondly, due to the mixture effects from tumor heterogeneity and edema, the reduced FA might not be solely attributed to white matter tract disruption. Future work considering the higher-order tensor could improve the estimation.

Conclusions

Glioblastoma causes widespread impairment to the brain structural connectome. The invisible disruption on conventional MRI and network integrity was correlated with patient survival. These global measures may provide a useful clinical tool for patient stratification and precise treatment.

Acknowledgment

Part of the data were obtained from the Alzheimer's Disease Neuroimaging Initiative (ADNI) database (adni.loni.usc.edu). As such, the investigators within the ADNI contributed to the design and implementation of ADNI and/or provided data but did not participate in the analysis or writing. The ADNI was launched in 2003 as a public-private partnership, led by Principal Investigator Michael W. Weiner, MD. A complete listing of investigators can be found at http://adni.loni.usc.edu/. For up-to-date information, see www.adni-info.org.

Data collection and sharing were funded by the Alzheimer's Disease Neuroimaging Initiative (ADNI) (National Institutes of Health Grant U01 AG024904) and DOD ADNI (Department of Defense award number W81XWH-12-2-0012). ADNI is funded by the National Institute on Aging, the National Institute of Biomedical Imaging and Bioengineering, and through generous contributions from the following: AbbVie, Alzheimer's Association; Alzheimer's Drug Discovery Foundation; Araclon Biotech; BioClinica, Inc.; Biogen; Bristol-Myers Squibb Company; CereSpir, Inc.; Cogstate; Eisai Inc.; Elan Pharmaceuticals, Inc.; Eli Lilly and Company; EuroImmun; F. Hoffmann-La Roche Ltd and its affiliated company Genentech, Inc.; Fujirebio; GE Healthcare; IXICO Ltd.; Janssen Alzheimer Immunotherapy Research & Development, LLC.; Johnson & Johnson Pharmaceutical Research & Development LLC.; Lumosity; Lundbeck; Merck & Co., Inc.; Meso Scale Diagnostics, LLC.; NeuroRx Research; Neurotrack Technologies; Novartis Pharmaceuticals Corporation; Pfizer Inc.; Piramal Imaging; Servier; Takeda Pharmaceutical Company; and Transition Therapeutics. The Canadian Institutes of Health Research is providing funds to support ADNI clinical sites in Canada. Private sector contributions are facilitated by the Foundation for the National Institutes of Health (www.fnih.org). The grantee organization is the Northern California Institute for Research and Education, and the study is coordinated by the Alzheimer's Therapeutic Research Institute at the University of Southern California. ADNI data are disseminated by the Laboratory for Neuro Imaging at the University of Southern California.

References

1. Davis ME. Glioblastoma: overview of disease and treatment. Clinical journal of oncology nursing **2016**;20(5):S2.
2. Scherer H. The forms of growth in gliomas and their practical significance. Brain **1940**;63(1):1-35.
3. Cuddapah VA, Robel S, Watkins S, Sontheimer H. A neurocentric perspective on glioma invasion. Nat Rev Neurosci **2014**;15(7):455-65 doi 10.1038/nrn3765.
4. Daniel AG, Park KY, Roland JL, Dierker D, Gross J, Humphries JB*, et al.* Functional connectivity within glioblastoma impacts overall survival. Neuro-Oncology **2020**.
5. Stoecklein VM, Stoecklein S, Galiè F, Ren J, Schmutzer M, Unterrainer M*, et al.* Resting-state fMRI detects alterations in whole brain connectivity related to tumor biology in glioma patients. Neuro-Oncology **2020** doi 10.1093/neuonc/noaa044.
6. Price S, Burnet N, Donovan T, Green H, Pena A, Antoun N*, et al.* Diffusion tensor Imaging of brain tumours at 3 T: A potential tool for assessing white matter tract invasion? Clinical Radiology **2003**;58(6):455-62 doi 10.1016/S0009-9260(03)00115-6.
7. Zikic D, Glocker B, Konukoglu E, Criminisi A, Demiralp C, Shotton J*, et al.* Decision forests for tissue-specific segmentation of high-grade gliomas in multi-channel MR. Med Image Comput Comput Assist Interv **2012**;15(Pt 3):369-76 doi 10.1007/978-3-642-33454-2_46.
8. Price SJ, Pena A, Burnet NG, Jena R, Green HA, Carpenter TA*, et al.* Tissue signature characterisation of diffusion tensor abnormalities in cerebral gliomas. Eur Radiol **2004**;14(10):1909-17 doi 10.1007/s00330-004-2381-6.
9. Hegi ME, Genbrugge E, Gorlia T, Stupp R, Gilbert MR, Chinot OL*, et al.* MGMT Promoter Methylation Cutoff with Safety Margin for Selecting Glioblastoma Patients into Trials Omitting Temozolomide: A Pooled Analysis of Four Clinical Trials. Clin Cancer Res **2019**;25(6):1809-16 doi 10.1158/1078-0432.CCR-18-3181.
10. Yan JL, Li C, Boonzaier NR, Fountain DM, Larkin TJ, Matys T*, et al.* Multimodal MRI characteristics of the glioblastoma infiltration beyond contrast enhancement. Ther Adv Neurol Disord **2019**;12:1756286419844664 doi 10.1177/1756286419844664.
11. Yan JL, Li C, Hoorn AV, Boonzaier NR, Matys T, Price SJ. A Neural Network Approach to Identify the Peritumoral Invasive Areas in Glioblastoma Patients by Using MR Radiomics. Sci Rep **2020**;10(1):9748 doi 10.1038/s41598-020-66691-6.
12. Price SJ, Allinson K, Liu H, Boonzaier NR, Yan JL, Lupson VC*, et al.* Less Invasive Phenotype Found in Isocitrate Dehydrogenase-mutated Glioblastomas than in Isocitrate Dehydrogenase Wild-Type Glioblastomas: A Diffusion-Tensor Imaging Study. Radiology **2017**;283(1):215-21 doi 10.1148/radiol.2016152679.
13. Li C, Wang S, Yan JL, Torheim T, Boonzaier NR, Sinha R*, et al.* Characterizing tumor invasiveness of glioblastoma using multiparametric magnetic resonance imaging. J Neurosurg **2019**:1-8 doi 10.3171/2018.12.JNS182926.
14. van Dijken BRJ, Yan JL, Boonzaier NR, Li C, van Laar PJ, van der Hoorn A*, et al.* Subventricular Zone Involvement Characterized by Diffusion Tensor Imaging in Glioblastoma. World Neurosurg **2017**;105:697-701 doi 10.1016/j.wneu.2017.06.075.
15. van Dijken BRJ, Jan van Laar P, Li C, Yan JL, Boonzaier NR, Price SJ*, et al.* Ventricle contact is associated with lower survival and increased peritumoral perfusion in glioblastoma. J Neurosurg **2018**;131(3):717-23 doi 10.3171/2018.5.Jns18340.

16. Crossley NA, Mechelli A, Scott J, Carletti F, Fox PT, McGuire P*, et al.* The hubs of the human connectome are generally implicated in the anatomy of brain disorders. Brain **2014**;137(8):2382-95 doi 10.1093/brain/awu132.
17. Raj A, LoCastro E, Kuceyeski A, Tosun D, Relkin N, Weiner M*, et al.* Network diffusion model of progression predicts longitudinal patterns of atrophy and metabolism in Alzheimer's disease. Cell reports **2015**;10(3):359-69.
18. Sun Y, Chen Y, Collinson SL, Bezerianos A, Sim K. Reduced Hemispheric Asymmetry of Brain Anatomical Networks Is Linked to Schizophrenia: A Connectome Study. Cerebral Cortex **2015**;27(1):602-15 doi 10.1093/cercor/bhv255.
19. Colon-Perez LM, Tanner JJ, Couret M, Goicochea S, Mareci TH, Price CC. Cognition and connectomes in nondementia idiopathic Parkinson's disease. Network Neuroscience **2018**;2(1):106-24.
20. Sporns O, Tononi G, Kötter R. The human connectome: a structural description of the human brain. PLoS Comput Biol **2005**;1(4):e42.
21. Bullmore E, Sporns O. Complex brain networks: graph theoretical analysis of structural and functional systems. Nature reviews neuroscience **2009**;10(3):186-98.
22. Rubinov M, Sporns O. Complex network measures of brain connectivity: uses and interpretations. Neuroimage **2010**;52(3):1059-69.
23. Yu Z, Tao L, Qian Z, Wu J, Liu H, Yu Y*, et al.* Altered brain anatomical networks and disturbed connection density in brain tumor patients revealed by diffusion tensor tractography. International journal of computer assisted radiology and surgery **2016**;11(11):2007-19.
24. Liu Y, Yang K, Hu X, Xiao C, Rao J, Li Z*, et al.* Altered rich-club organization and regional topology are associated with cognitive decline in patients with frontal and temporal gliomas. Frontiers in human neuroscience **2020**;14:23.
25. Aerts H, Fias W, Caeyenberghs K, Marinazzo D. Brain networks under attack: robustness properties and the impact of lesions. Brain **2016**;139(12):3063-83.
26. Liu L, Zhang H, Rekik I, Chen X, Wang Q, Shen D. Outcome prediction for patient with high-grade gliomas from brain functional and structural networks. 2016. Springer. p 26-34.
27. Squarcina L, Bertoldo A, Ham TE, Heckemann R, Sharp DJ. A robust method for investigating thalamic white matter tracts after traumatic brain injury. Neuroimage **2012**;63(2):779-88.
28. Schult T, Hauser T-K, Klose U, Hurth H, Ehricke H-H. Fiber visualization for preoperative glioma assessment: Tractography versus local connectivity mapping. Plos one **2019**;14(12):e0226153.
29. Miller P, Coope D, Thompson G, Jackson A, Herholz K. Quantitative evaluation of white matter tract DTI parameter changes in gliomas using nonlinear registration. Neuroimage **2012**;60(4):2309-15.
30. Sinha R, Dijkshoorn AB, Li C, Manly T, Price SJ. Glioblastoma surgery related emotion recognition deficits are associated with right cerebral hemisphere tract changes. Brain communications **2020**;2(2):fcaa169.
31. Wang X, Zhou C, Wang L, Wang Y, Jiang T. Motor cortex gliomas induces microstructural changes of large fiber tracts revealed by TBSS. Scientific Reports **2020**;10(1):1-8.

32. Park C-h, Kou N, Boudrias M-H, Playford ED, Ward NS. Assessing a standardised approach to measuring corticospinal integrity after stroke with DTI. NeuroImage: clinical **2013**;2:521-33.
33. Griffis JC, Metcalf NV, Corbetta M, Shulman GL. Structural disconnections explain brain network dysfunction after stroke. Cell reports **2019**;28(10):2527-40. e9.
34. Fagerholm ED, Hellyer PJ, Scott G, Leech R, Sharp DJ. Disconnection of network hubs and cognitive impairment after traumatic brain injury. Brain **2015**;138(6):1696-709.
35. Smith SM, Jenkinson M, Johansen-Berg H, Rueckert D, Nichols TE, Mackay CE*, et al.* Tract-based spatial statistics: voxelwise analysis of multi-subject diffusion data. Neuroimage **2006**;31(4):1487-505.
36. Jolly AE, Scott GT, Sharp DJ, Hampshire AH. Distinct patterns of structural damage underlie working memory and reasoning deficits after traumatic brain injury. Brain **2020**;143(4):1158-76.
37. Gorlia T, van den Bent MJ, Hegi ME, Mirimanoff RO, Weller M, Cairncross JG*, et al.* Nomograms for predicting survival of patients with newly diagnosed glioblastoma: prognostic factor analysis of EORTC and NCIC trial 26981-22981/CE. 3. The lancet oncology **2008**;9(1):29-38.
38. Jenkinson M, Bannister P, Brady M, Smith S. Improved optimization for the robust and accurate linear registration and motion correction of brain images. Neuroimage **2002**;17(2):825-41.
39. Kamnitsas K, Ferrante E, Parisot S, Ledig C, Nori AV, Criminisi A*, et al.* DeepMedic for brain tumor segmentation. 2016. Springer. p 138-49.
40. Tzourio-Mazoyer N, Landeau B, Papathanassiou D, Crivello F, Etard O, Delcroix N*, et al.* Automated anatomical labeling of activations in SPM using a macroscopic anatomical parcellation of the MNI MRI single-subject brain. Neuroimage **2002**;15(1):273-89.
41. Grabner G, Janke AL, Budge MM, Smith D, Pruessner J, Collins DL. Symmetric atlasing and model based segmentation: an application to the hippocampus in older adults. 2006. Springer. p 58-66.
42. Avants BB, Tustison N, Song G. Advanced normalization tools (ANTS). Insight j **2009**;2(365):1-35.
43. Behrens TE, Berg HJ, Jbabdi S, Rushworth MF, Woolrich MW. Probabilistic diffusion tractography with multiple fibre orientations: What can we gain? Neuroimage **2007**;34(1):144-55.
44. Andersson JL, Sotiropoulos SN. An integrated approach to correction for off-resonance effects and subject movement in diffusion MR imaging. Neuroimage **2016**;125:1063-78.
45. Andersson JL, Jenkinson M, Smith S. Non-linear registration aka Spatial normalisation FMRIB Technial Report TR07JA2. FMRIB Analysis Group of the University of Oxford **2007**:1-22.
46. Schwarz CG, Reid RI, Gunter JL, Senjem ML, Przybelski SA, Zuk SM*, et al.* Improved DTI registration allows voxel-based analysis that outperforms tract-based spatial statistics. Neuroimage **2014**;94:65-78.
47. Ou Y, Akbari H, Bilello M, Da X, Davatzikos C. Comparative evaluation of registration algorithms in different brain databases with varying difficulty: results and insights. IEEE transactions on medical imaging **2014**;33(10):2039-65.

48. Prasanna P, Mitra J, Beig N, Nayate A, Patel J, Ghose S, *et al.* Mass Effect Deformation Heterogeneity (MEDH) on Gadolinium-contrast T1-weighted MRI is associated with decreased survival in patients with right cerebral hemisphere Glioblastoma: A feasibility study. Scientific reports **2019**;9(1):1-13.
49. Nyúl LG, Udupa JK, Zhang X. New variants of a method of MRI scale standardization. IEEE transactions on medical imaging **2000**;19(2):143-50.
50. Watts DJ, Strogatz SH. Collective dynamics of 'small-world'networks. nature **1998**;393(6684):440-2.
51. Lin H, Zelterman D. Modeling survival data: extending the Cox model. Taylor & Francis; 2002.
52. 2020 March 3, 2021. VASARI Research Project. <https://wiki.cancerimagingarchive.net/display/Public/VASARI+Research+Project>. March 3, 2021.
53. Barajas RF, Jr, Phillips JJ, Parvataneni R, Molinaro A, Essock-Burns E, Bourne G, *et al.* Regional variation in histopathologic features of tumor specimens from treatment-naive glioblastoma correlates with anatomic and physiologic MR Imaging. Neuro-Oncology **2012**;14(7):942-54 doi 10.1093/neuonc/nos128.
54. Sporns O, Zwi JD. The small world of the cerebral cortex. Neuroinformatics **2004**;2(2):145-62.